A&A 375, 950–962 (2001)
DOI: 10.1051/0004-6361:20010878

Astronomy & Astrophysics

Processing of silicate dust grains in Herbig Ae/Be systems

J. Bouwman[1], G. Meeus[2], A. de Koter[1], S. Hony[1], C. Dominik[1], and L. B. F. M. Waters[1,2]

[1] Astronomical Institute "Anton Pannekoek", University of Amsterdam, Kruislaan 403, 1098 SJ Amsterdam, The Netherlands
[2] Instituut voor Sterrenkunde, K.U. Leuven, Celestijnenlaan 200 B, 3001 Heverlee, Belgium

Received 2 February 2001 / Accepted 15 June 2001

Abstract. We have analysed the 10 μm spectral region of a sample of Herbig Ae/Be (HAEBE) stars. The spectra are dominated by a broad emission feature caused by warm amorphous silicates, and by polycyclic aromatic hydrocarbons. In HD 163296 we find aliphatic carbonaceous dust, the first detection of this material in a HAEBE star. The silicate band shows a large variation in shape, due to variable contributions of three components: (i) a broad shoulder at 8.6 μm; (ii) a broad maximum at 9.8 μm; and (iii) a narrow feature with a broad underlying continuum at 11.3 μm. From detailed modeling these features can be identified with silica (SiO_2), sub-micrometer sized amorphous olivine grains and micrometer sized amorphous olivine grains in combination with forsterite (Mg_2SiO_4), respectively. Typical mass fractions are 5 to 10 per cent of crystalline over amorphous olivine, and a few per cent of silica compared to the olivines. The detection of silica in emission implies that this material is heated by thermal contact with other solids that have a high absorptivity at optical to near-IR wavelengths. The observed change in peak position of the silicate band in HAEBE stars from 9.7 μm to 11.3 μm is dominated by an increase in average grain size, while changes in composition play only a minor rôle. The HAEBE stars, β Pic and the solar system comet Halley form a sequence of increasing crystallinity. We find that the abundance of SiO_2 tends to increase with increasing crystallinity. This is consistent with the compositional changes expected from thermal annealing of amorphous grains in the inner regions of the disk. We confirm earlier studies that the timescale for crystallisation of silicates in disks is longer than that of coagulation. Our results indicate that the processes that governed grain processing in the proto-solar nebula, are also at work in HAEBE stars.

Key words. circumstellar matter – stars: formation – stars: pre-main-sequence

1. Introduction

This paper is one in a series in which we study the circumstellar environment around Herbig Ae/Be (HAEBE) systems as observed with the Short Wavelength Spectrometer (SWS; de Graauw et al. 1996) on board of the Infrared Space Observatory (ISO; Kessler et al. 1996). HAEBE stars represent the final stage of pre-main-sequence (PMS) evolution of intermediate-mass stars ($\sim$2–10 $M_\odot$). As a consequence of the star formation process these stars are typically surrounded by a gas and dust envelope and/or disk. They may be the precursors of young main sequence β-Pictoris and Vega-type stars (see Waters & Waelkens 1998 for a review). These latter systems are surrounded by circumstellar debris disks, which perhaps contain planetary bodies (e.g. Aumann et al. 1984; Beust et al. 1996). This would imply that the environment around HAEBE stars represents an early phase in the formation of planets. Millimetre interferometry and observations in CO emission lines show indeed disks around a number of these stars (Mannings & Sargent 1997, 2000). Furthermore, infalling circumstellar gas observed in a number of HAEBE systems with similar characteristics as in the β-Pic system, is consistent with infalling and evaporating planetesimals (Grady et al. 1997, 1999). ISO spectroscopy of isolated HAEBE stars has also strengthened the link between HAEBE stars and planet formation. Analysis of the ISO-SWS and Long Wavelength Spectrometer (LWS; Clegg et al. 1996) spectra of HD 142527 revealed the presence of hydrated silicates (Malfait et al. 1999). These types of silicates are also found in a major fraction of interplanetary dust particles (IDPs; Sandford & Walker 1985). The remarkable similarity between the ISO spectrum of the Herbig Be star HD 100546 and the solar system comet C/1995 O1 (Hale-Bopp; Crovisier et al. 1997; Malfait et al. 1998b), both showing a high abundance of crystalline silicates and similar dust composition, also strengthens the interpretation of HAEBE stars as sites of planet formation.

Here we want to study the compositional properties of the circumstellar disks of HAEBE stars. We have therefore selected isolated objects, i.e. not inside a star forming region, such that confusion with other sources is minimised. Our sample consists of 14 objects which are

Send offprint requests to: J. Bouwman,
e-mail: jeroenb@astro.uva.nl

observed with ISO-SWS in mode AOT1. The spectra were reduced in a standard way using the ISO-SWS Interactive Analysis (IA) tool and the ISO Spectral Analysis Package (ISAP). For a detailed description of the observations we refer to Meeus et al. (2001, hereafter Paper I). The ISO spectra of a number of stars in our sample, HD 100546 (Malfait et al. 1998b), HD 142527 (Malfait et al. 1999), HD 163296 & AB Aur (van den Ancker et al. 2000; Bouwman et al. 2000, hereafter B2000) have been presented and analysed in previous studies. This, however, is the first time that a compositional analysis of the entire ISO sample of isolated HAEBE stars is made. Using a simple and identical analysis method for the entire sample, the derived grain composition of the individual systems can be compared directly. This enables us to determine a sequence in the amount of silicate grain processing.

In Paper I, we presented the infrared spectra of our sample and made a classification into two groups depending on the shape of the spectral energy distribution (SED). We suggested an explanation for the difference between the groups in terms of disk geometry and grain size. In this paper we focus on the silicate grain processing in these systems (making up the bulk of the dust) and give a quantitative analysis of the observed solid state emission. We focus our analysis on the 10 μm spectral region, the main reasons being the occurrence of strong silicate resonances and the possibility of making a good estimate of the emission of other solid state species in this region. The emission in this region is dominated by grains with temperatures in the range of ∼500–1000 K. These temperatures are reached in the inner parts of the protoplanetary disks. The derived dust composition is thus representative for the silicate dust within ∼10 AU from the central star.

This paper is organised in the following way: in Sect. 2 we will introduce the main dust components and the method used to analyse the ISO spectra. In Sect. 3 modelling results are presented and in Sect. 4 we will discuss results and inferences for the evolution of the dust in the circumstellar environment of HAEBE stars.

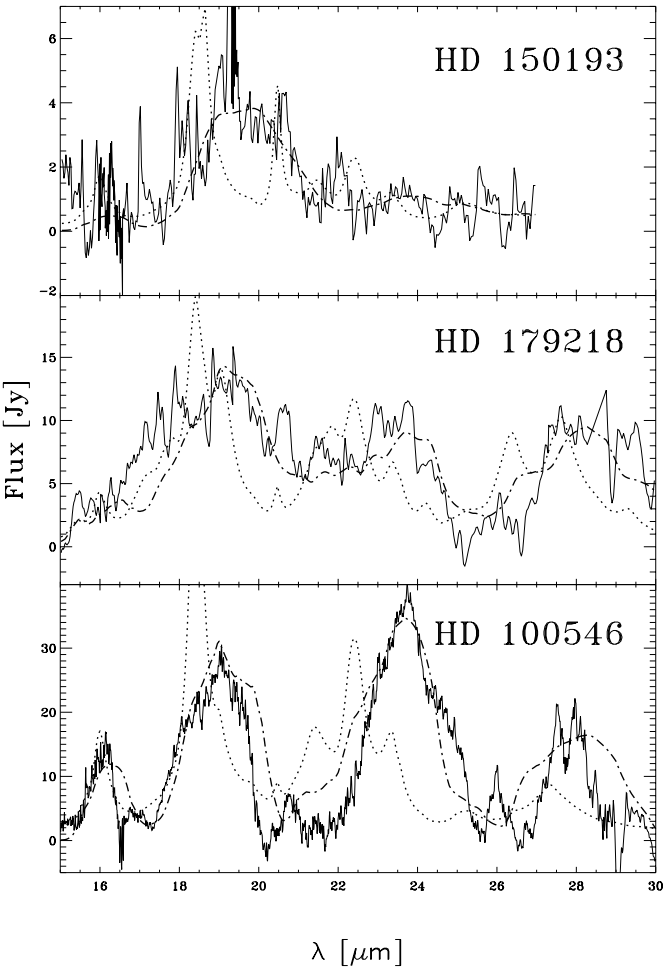

Fig. 1. The emission features due to crystalline silicates in the spectra of HD 150193 (top), HD 179218 (middle), and HD 100546 (bottom). The dashed-dotted lines indicate our best fits to the continuum subtracted spectra using a continuous distribution of ellipsoids; dotted lines are best fit models assuming spheres. The CDE distribution yields by far the best fit result.

2. Dust composition and spectral analysis

2.1. Adopted dust components and grain shapes

In order to arrive at a sensible choice of dust components and grain shapes, we use the outcome of detailed radiative transfer analysis on two of our programme stars, HD 163296 and AB Aur. The stars show a similar dust composition with the near-IR and mid-IR dominated by solid state emission from small grains, with sizes between 0.01 and ∼5 μm (B2000). The bulk of the material (∼70%) consists of amorphous iron magnesium silicates (olivine) dominating the 10 and 18 μm region. The near-IR fluxes are mainly due to iron or iron-oxides and carbonaceous grains which make up ∼15% of the total mass. HD 163296 also shows emission bands due to crystalline magnesium silicate (forsterite) grains. Similar results are found for HD 142527 and HD 100546 (Malfait et al. 1998b, 1999; Bouwman et al. in prep) although the latter system is found to have much higher abundances of crystalline silicates. In this study we will focus on the silicate dust component and will subtract the smooth contributions from other (metallic iron, iron-oxide, carbon) dust species (see Sect. 2.2).

The residue spectrum of HD 163296, obtained by subtracting the observed ISO-SWS spectrum from our best radiative transfer model fit (B2000), revealed an emission component at ∼8.6 μm not included in the dust composition adopted by B2000, which we tentatively attribute to silica. The presence of silica in the circumstellar dust around HAEBE stars is suggested by the presence of large silica grains in interplanetary dust particles (Rietmeijer 1988). Thermal annealing experiments of magnesium silicate smokes show that during the annealing process silica can form together with forsterite (Rietmeijer et al. 1986; Hallenbeck & Nuth 1997; Fabian et al. 2000). Another possibility to form silica is the reduction of iron-rich silicate

grains by H_2 (Allen et al. 1993). The dust components we use in this study are listed in Table 1 together with the grain composition, size, shape distribution and bulk density.

We investigated the sensitivity of the spectroscopic signature of the grains to changes in particle shape and size. Shape effects were studied by comparing predictions for spherical grains (Mie theory), ellipsoidal grains of the same form, and a continuous distribution of ellipsoids (CDE; see Bohren & Huffman 1983 for a review on these methods). The calculations for ellipsoids were performed in the Rayleigh limit, which yields spectroscopic properties independent of grain size.

The amorphous olivine grains show little dependence on shape, but display a strong dependence on size. In general, for larger grains the contrast of a feature relative to the continuum becomes less, especially when the grains have radii $a > 2$ μm. By comparing the optical properties of these particles, assuming they are spheres, for the size range which dominates the 10 μm silicate feature (0.01 to $\sim$5 μm), we find that the emission can be characterised by two typical grain sizes: 0.1 μm for grains with sizes <1 μm, and 2 μm for grains >1 μm. We will investigate the contribution of small and large particles on the emission properties of olivine grains by adopting these two typical sizes.

Contrary to the amorphous olivine, the spectroscopic properties of crystalline silicates are very sensitive to the adopted grain shape. Before discussing this, we mention that also the chemical composition of these grains strongly affects the emission features, specifically the Fe over Mg ratio. Detailed analysis of disk sources has shown that the crystalline silicates of the olivine and pyroxene family are pure or nearly pure magnesium silicates (e.g. Molster et al. 1999a). Here we will assume that these crystals are the pure magnesium silicates forsterite (Mg_2SiO_4) and/or enstatite ($MgSiO_3$). To determine the shape of the silicate crystals we fitted the multiple features of forsterite and enstatite in the 15 to 30 μm range in the continuum subtracted spectra of HD 150193, HD 179218 and HD 100546. These stars display the most prominent crystalline bands. Figure 1 shows these spectra. The continuum subtracted spectrum of HD 150193 is dominated by emission from SiO_2 grains, giving rise to an emission complex around 20 μm. The spectrum of HD 100546 is dominated by forsterite emission, while HD 179218 also shows features due to enstatite. The figure also shows the best fit to the silicate bands for different shape properties. We obtained emissivities by multiplying the absorption coefficients with two black bodies of 350 and 80 K respectively, which gave the best fit to the entire wavelength range. This simplified representation of a temperature distribution does not significantly affect our conclusions with respect to particle shape. These conclusions are that spherical grains fail in predicting the correct peak positions as well as in producing the width of the features (they are too narrow). Ellipsoidal grains on the other hand produce a fair match to both the location and the width of the features, the best results being achieved using the CDE distribution. We therefore adopted CDE for our modelling effort. As we treat the CDE particles in the Rayleigh limit, we can not study grain size effects. However, in analogy with spherical grains we anticipate a diminishing contrast of the features when $a > 2$ μm. The calculated optical properties of the dust species adopted are listed in Table 1 and are plotted in Fig. 2.

Table 1. The grain species used to fit the ISO-SWS spectra. Listed are composition, grain size, assumed shape, and bulk density of the material.

Species	Composition	Size [μm]	Shape	ρ_b [grcm^{-3}]
Olivine[1]	$[Mg,Fe]_2SiO_4$	0.1 & 2.0	Spheres	3.71
Forsterite[2]	Mg_2SiO_4	0.1	CDE	3.33
Enstatite[3]	$MgSiO_3$	0.1	CDE	2.80
Silica[4]	SiO_2	0.1	CDE	2.21

Ref.: (1) Dorschner et al. (1995); (2) Servoin & Piriou (1973); (3) Jäger et al. (1998); (4) Spitzer & Kleinman (1961).

2.2. Spectral analysis

To determine the composition of the circumstellar dust in the HAEBE systems, we construct model profiles by making linear combinations of the absorption profiles of the adopted dust species. The resulting model profile is given by

$$\kappa_{\rm model}(\lambda) = \sum_i a_i \kappa_i(\lambda) \quad (1)$$

where $\kappa_i(\lambda)$ are the absorption profiles of the dust species listed in Table 1 and a_i the multiplication factors which are listed in Table 2. We have several reasons for applying this relatively simple modeling approach. It is clearly a completely valid method if the dust medium is optically thin, as suggested by the fact that all observed solid state features are in emission. Still relatively modest line-of-sight self shielding effects may play a role, which would require full 2-dimensional radiative transfer modeling to properly sort out. However, our approach is to first gain a better understanding of the general qualitative trends in grain composition, shape and processing observed in the ISO spectra. These results may then help in constraining parameter space when making detailed 2D modeling efforts. We note that preliminary full 2D computations of disk emission using identical dust composition as for the optically thin model show that the results presented in this paper are in qualitative agreement, which adds to the validity of the present approach (Bouwman et al., in preparation).

We focus on the region centered around 10 μm because one of the main resonances of the amorphous silicates is located at $\sim$9.8 μm. Within the wavelength range

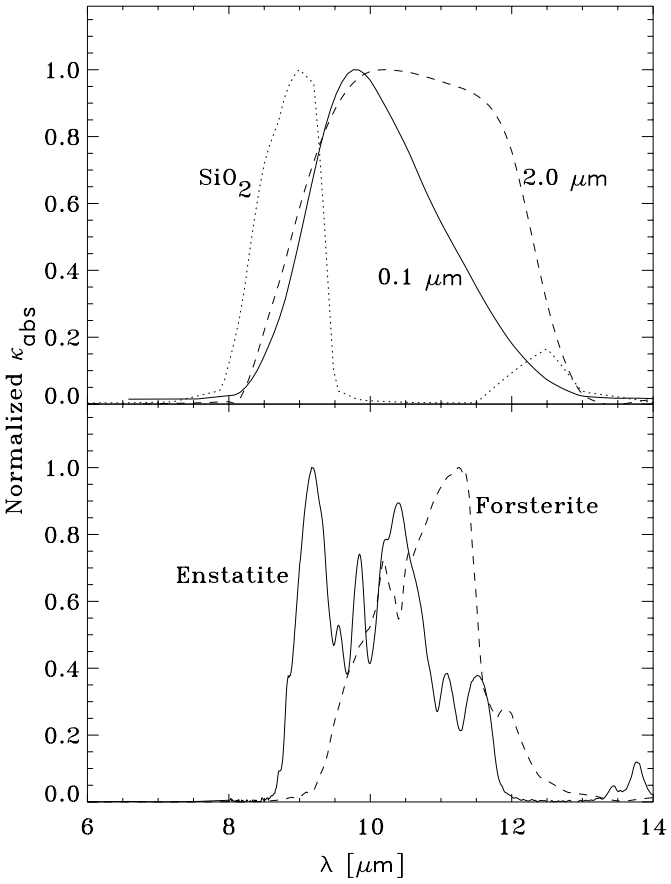

Fig. 2. The emission properties of silicate dust grains. Plotted are the normalised absorption coefficients against wavelength. The top panel shows the absorption coefficients of quartz and amorphous olivine for two grain sizes. The bottom panel shows the crystalline dust species enstatite and forsterite. The normalizing constants in cm^2 gr^{-1} for the silica, 0.1 and 2.0 μm amorphous olivine are 3.5×10^3, 1.7×10^3 and 2.2×10^4, respectively. For enstatite and forsterite the normalisation is 7.3×10^3 and 7.6×10^3, respectively.

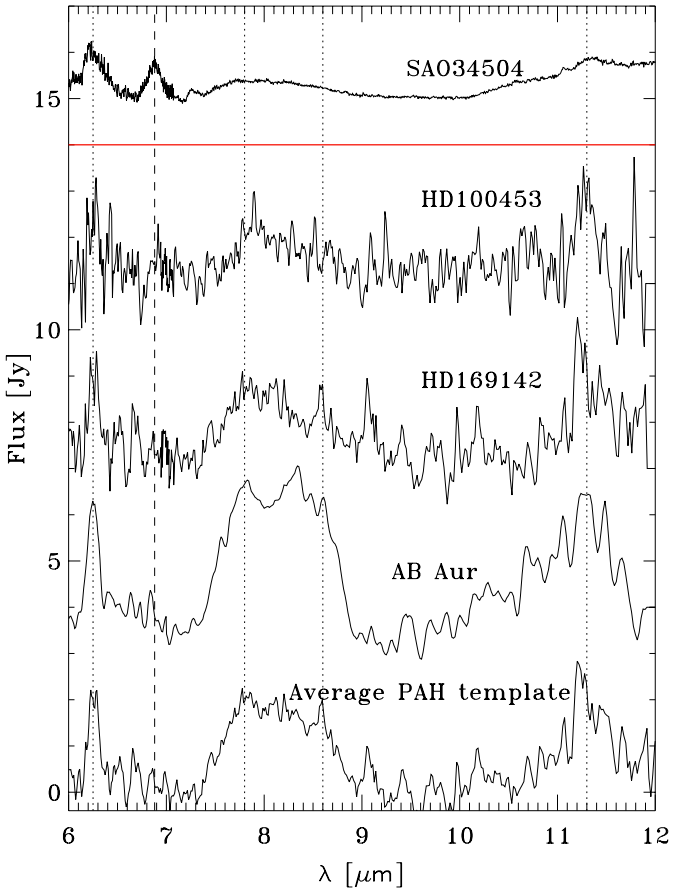

Fig. 3. The infrared emission bands of PAHs and aliphatic hydrocarbons. Plotted are the continuum subtracted spectra of SAO 34504, HD 100453 and HD 169142 and the model subtracted spectra of AB Aur. Indicated in the figure are the bands at 6.25, 7.8, 8.6 and 11.3 μm due to PAHs (dotted lines) and the 6.9 μm band due to aliphatic hydrocarbons (dashed line). The bottom curve shows the template spectrum used to estimate the relative PAH contributions.

from 6 to 14 μm a clear distinction between the emission from silicate dust grains and other dust species producing a smooth continuum can be made, allowing us to subtract the smooth continuum contribution (see previous section). This distinction is problematic when using the other main resonance of the amorphous silicates near 18 μm, where resonances from other dust species such as iron-magnesium oxides or iron sulfides are important. Often this resonance is located on the edge of a rising continuum caused by the cold bulk material present in these HAEBE systems, making it difficult to determine the shape and strength of the 18 μm band. This makes it impossible to determine the amount of amorphous silicate dust. A meaningful fit to these longer wavelengths can only be made by applying a full radiative transfer method. It is important to realize that the choice of the 10 μm region implies that the derived dust compositions are representative only for the inner parts of the protoplanetary disks in the HAEBE systems.

One of the difficulties in fitting the silicate features is that the main resonance of forsterite at 11.3 μm (shown in Fig. 2) coincides with a strong emission feature usually attributed to polycyclic aromatic hydrocarbons (PAHs; Allamandola, Bark, Tielens 1989). PAH emission is observed in a large fraction of our sample of HAEBE systems (see Paper I). To determine the band strength of forsterite we first have to make an estimate of the PAH emission at 11.3 μm. We have three objects where we know the contribution from PAHs well; these are shown in Fig. 3. Marked in this figure are the PAH bands near 6.2, 7.8, 8.6 and 11.3 μm. Both HD 100453 and HD 169142 do not show any emission due to silicates, so a direct determination of the PAH band strength is possible. AB Aur does show silicate emission, but only from amorphous material, which has resonances much broader than the PAH bands. From detailed modelling (B2000) we can determine the silicate contribution, which we subtracted from the ISO-SWS spectra.

The position and relative band strengths of the 6.2 and 11.3 μm bands for all three sources are equal within the error margins. We determined an average spectrum of the three sources and used this as a template to determine the PAH contribution in the other HAEBE systems. This template spectrum is also shown in Fig. 3. To estimate the PAH contribution at 11.3 μm, we scale the PAH template spectrum to the strength of the 6.2 μm feature, which is clearly visible and well isolated, such that contamination effects are minimised. We use the template spectrum as a separate spectral component in the fits presented in Sect. 3.

2.3. Detection of aliphatic hydrocarbons in HD 163296

One system, HD 163296, shows a band at 6.9 μm due to aliphatic hydrocarbons, which is the first detection of this species in a HAEBE system (Hony et al. in prep.). These types of hydrocarbons are likely to be incorporated into grains unlike the PAHs (e.g. Guillois et al. 1996). It is clear that for HD 163296 we cannot use the PAH template, and we must find other objects with aliphatic bands to serve as a template. The carbon-rich post-asymptotic giant branch star SAO 34504 has one of the most pronounced 6.9 μm bands observed in any evolved carbon-rich star (Fig. 3), and we use its spectrum as a template for HD 163296. Note that the position and shape of the bands in SAO 34504 are quite different from those of the PAH template. We adopt a temperature of 250 K for the aliphatic carbonaceous dust, derived from the 6.2 to 6.9 μm band strength ratio in HD 163296.

3. Results

Figure 4 shows the continuum subtracted spectra of the programme stars. Of the four stars that do not show any silicate emission bands we only plot HD 100453 and HD 169142, as these are the only ones that do show PAH features. We have also included some comparison spectra of other objects showing the 10 μm band. The idea is that these reference objects provide limiting cases for the composition of the dust in the HAEBE systems. The silicate profile of the ISM, observed with ISO in the direction of Sgr A (Kemper et al. 2001, in prep.), shows the material in the form in which it is expected to be present during the first phases of star and disk formation. The spectrum of the red supergiant μ Cep is representative for this class of objects and shows dust with remarkably similar properties as the silicates in the ISM. Contrasting these cases where only amorphous silicate dust material is observed, we also show three cases in which the dust is expected to be highly processed.

The spectra of the comets Hale-Bopp and 1P/Halley show the end results of processing of solar system dust grains before being incorporated into cometary bodies. These types of grains may be representative for the late stages of dust evolution in the protoplanetary disks around HAEBE stars. The spectrum of Halley shown here was observed when the comet was at a heliocentric distance of 1.3 AU (Bregman et al. 1987). We show two spectra of Hale-Bopp, one observed in October 1996, when the object was a 2.8 AU (Crovisier et al. 1997), and one observed in April 1997, when it was at a distance of 0.97 AU (Hayward et al. 2000). Also representative for the late stages of dust evolution in protoplanetary disks may be the spectrum of β Pictoris (Pantin et al. 1999), which has a collisionally dominated debris disk and may be an end stage of HAEBE evolution.

The spectra in Fig. 4 are ordered (from top to bottom, left to right) according to the peak-position of the silicate feature. The feature shifts from 9.8 μm, the peak position of the ISM silicate band and indicated with the dashed line, towards 11.3 μm. The latter wavelength corresponds to one of the strongest resonances of forsterite and a PAH band (see Figs. 2 and 3). Apart from this shift in peak-position the silicate band also broadens and changes shape from a steep blue wing with a slow red decline towards a profile which is slowly rising and then drops steeply. To quantify these trends in peak position, width and skewness we measured the excess flux above continuum at 8.6, 9.8 and 11.3 μm. These positions correspond to the shoulder of the silicate feature at short wavelengths, the shortest wavelength of the peak position and the longest wavelength of the peak position, respectively.

In Fig. 5 we show the correlations between the ratios of the excess fluxes at 8.6, 9.8 and 11.3 μm, after removing the PAH contributions. In this and following figures the HAEBE stars are represented with filled symbols while the reference objects are indicated with open symbols. The diamond, upside down triangle, star, and circles represent the ISM, μ Cep, β Pic, and the comets, respectively. Note that the flux ratio $F_{8.6}/F_{11.3}$ is fairly constant for the HAEBE stars at $\sim$0.45, except for three objects. We have marked the HAEBE systems with a $F_{8.6}/F_{11.3}$ flux ratio of $\sim$0.45 with a larger symbol. The exceptions are HD 100546 (marked with 2) and the reference object Hale-Bopp (two observations marked with 1), showing a ratio about twice as small, and HD 150193 (marked with 3) which has this ratio a factor of two larger. Leaving out these exceptions, one finds a reasonably tight correlation between the 8.6 over 9.8 and the 11.3 over 9.8 μm flux ratios. We fitted a relation of the form $Y = aX^b$, resulting in $b = 0.93 \pm 0.23$ and $a = 0.43 \pm 0.03$ (dotted line in top panel). We will return to the exceptions in Sect. 4; for the moment we exclude these objects from the correlation analysis we discuss below.

Overplotted in Fig. 4 are our best fits, using the analysis method described above. The results of our fitting procedure are listed in Table 2. The first column lists the spectral type of the HAEBE stars in our sample, and μ Cep and β Pic (Malfait et al. 1998b; Dunkin et al. 1997; Gray & Corbally 1998; Kukarkin et al. 1971), while columns three to six give the multiplication factors of the absorption coefficients of the included dust species. The derived mass ratios of the dust components used in our fit are listed in column seven to nine. Column 7 lists the mass ratio of the

Table 2. Model fit parameters for the sample of HAEBE stars and reference objects. Columns 1 and 2 give the name of the object and its spectral type when applicable; Cols. 3 to 6 list the multiplication factors of the individual dust components (Eq. (1)), used to make a linear contribution of the in Fig. 2 plotted absorption coefficients. Columns 7 to 9 list the derived mass ratios between the 2.0 and 0.1 μm amorphous olivine grains $m_{2.0}/m_{0.1}$, between forsterite and the total mass of the silicates $m_{\rm forst}/m_{\rm sil}$ and between SiO_2 and all silicates $m_{\rm SiO_2}/m_{\rm sil}$ respectively. Column 10 shows the strength of the PAH emission relative to the template spectrum.

(1)	(2)	(3)	(4)	(5)	(6)	(7)	(8)	(9)	(10)
	Spectral	Amorphous Olivine							
Source	Type	0.1 μm	2.0 μm	Forsterite	SiO_2	$m_{2.0}/m_{0.1}$	$m_{\rm forst}/m_{\rm sil}$	$m_{\rm SiO_2}/m_{\rm sil}$	PAH
Gal Centre.		2500	<0.013	<30	<40	<0.04	$<0.011^c$	$<9.3\times10^{-3\,c}$	<0.01
μ Cep	M2e Ia	6.5×10^5	35	<200	<8000	0.43	$<0.019^d$	$<5.0\times10^{-3\,d}$	<1.0
AB Aur	B9/A0Ve	10 000	1.25	<100	<50	1.0	$<4.5\times10^{-3\,d}$	$<1.5\times10^{-3\,d}$	1.0
HD 150193	A1Ve	7000	0.25	500	800	0.29	0.045	0.048	<0.1
HD 163296	A3Ve	9500	0.5	600	500	0.42	0.038	0.021	0.04^b
HD 144432	A9Ve	2800	0.3	475	150	0.86	0.075	0.016	<0.05
HD 142666	A8Ve	1300	0.25	50	80	1.54	0.013	0.014	0.4
Hale Bopp April 97		13 000	0.25	7000	750	0.15	0.29	0.021	<0.1
51 Oph	A0Ve	1500	0.63	150	100	3.33	0.020	8.9×10^{-3}	<0.04
HD 104237	A4Ve	1000	1.0	800	400	8	0.072	0.024	<0.05
HD 142527	F7IIIe	500	1.0	600	400	16	0.058	0.026	0.6
β-Pic	A5V	220	0.11	230	70	3.9	0.16	0.031	<0.005
Halley		11 000	3.75	13 500	3000	2.73	0.22	0.033	<0.05
HD 179218	B9e	2800	1.0	1400^a	500	2.86	0.092^a	0.022	2.5
HD 100546	B9Ve	<600	4.25	6200	<300	>57	0.14^e	$<4.5\times10^{-3\,e}$	3.8
Hale Bopp Oct. 96		9500	0.5	10 000	400	0.42	0.40	0.011	<0.1
HD 100453	A9Ve	<50	<0.025	<10	<20	–	–	–	0.7
HD 169142	A5Ve	<50	<0.025	<10	<10	–	–	–	0.9
HD 139614	A7Ve	<80	<0.05	<10	<10	–	–	–	<0.05
HD 135344	F4Ve	<10	<0.0125	<10	<10	–	–	–	<0.05

Notes: ^{a} HD 179218 has a substantial contribution from enstatite. The multiplication factor is 1400.0 resulting in a total mass fraction of crystalline magnesium silicates of 0.17; ^{b} We used the SAO 34504 template to fit the emission by aliphatic hydrocarbons assuming a grain temperature of 250 K; ^{c} We used $m_{\rm sil} = m_{0.1}$; ^{d} We used $m_{\rm sil} = m_{0.1}+m_{2.0}$; ^{e} We used $m_{\rm sil} = m_{2.0}+m_{\rm forst}$.

2.0 over 0.1 μm amorphous olivine grains, column eight the mass ratio of forsterite over the total silicate mass, and column nine the mass fraction of silica.

3.1. Correlations

To link the derived dust composition with the observed changes in the 10 μm silicate feature, we compared the mass ratios as listed in Table 2 with the flux ratios used in Fig. 5a. Plotted in Fig. 6a is the ratio between mass contained in large amorphous grains ($a = 2$ μm) and small amorphous grains ($a = 0.1$ μm). This ratio is indicative for the typical grain size. In panel b of the same figure we show the forsterite mass fraction (relative to the total silicate mass), and in panel c the silica mass fraction. All three quantities are plotted as a function of the 11.3 over 9.8 μm flux ratio, which provides a measure for the peak position of the 10 μm silicate feature, which varies between 9.8 and 11.3 μm as can be seen in Fig. 4. The dotted line represents a least square fit to the objects selected on grounds of their 8.6 over 11.3 μm flux ratio. In fitting this and all other correlations presented in this paper, HD 100546 and HD 150193 are always excluded. Also excluded will be objects for which in the correlation being discussed only upper/lower limits are available. Objects not taken into account have been given a small symbol size for clarity. In figures where no correlation can be found we have not used this convention.

For the HAEBE systems a strong correlation can be seen between the grain size of the amorphous iron magnesium silicates, producing the bulk of the emission, and the peak position of the silicate feature. Fitting the same relation as in Fig. 5a yields $b = 3.96 \pm 0.08$ $a = 4.89 \pm 0.05$. This strong dependence on grain size of the 11.3 over 9.8 μm flux ratio is a reflection of the emission properties of the amorphous olivine as shown in Fig. 2. An increase in grain size results in a large increase of the 11.3 μm flux relative to the 9.8 μm flux. Notice that all solar system objects and β Pic fall beneath the derived correlation for the HAEBE systems.

In Fig. 6b we show the relation between the peak position of the silicate band and the mass fraction of forsterite. Since forsterite has a strong resonance at 11.3 μm, it is expected that a high mass fraction of forsterite will also shift the peak to longer wavelength. We caution that the determination of the forsterite mass fraction suffers from

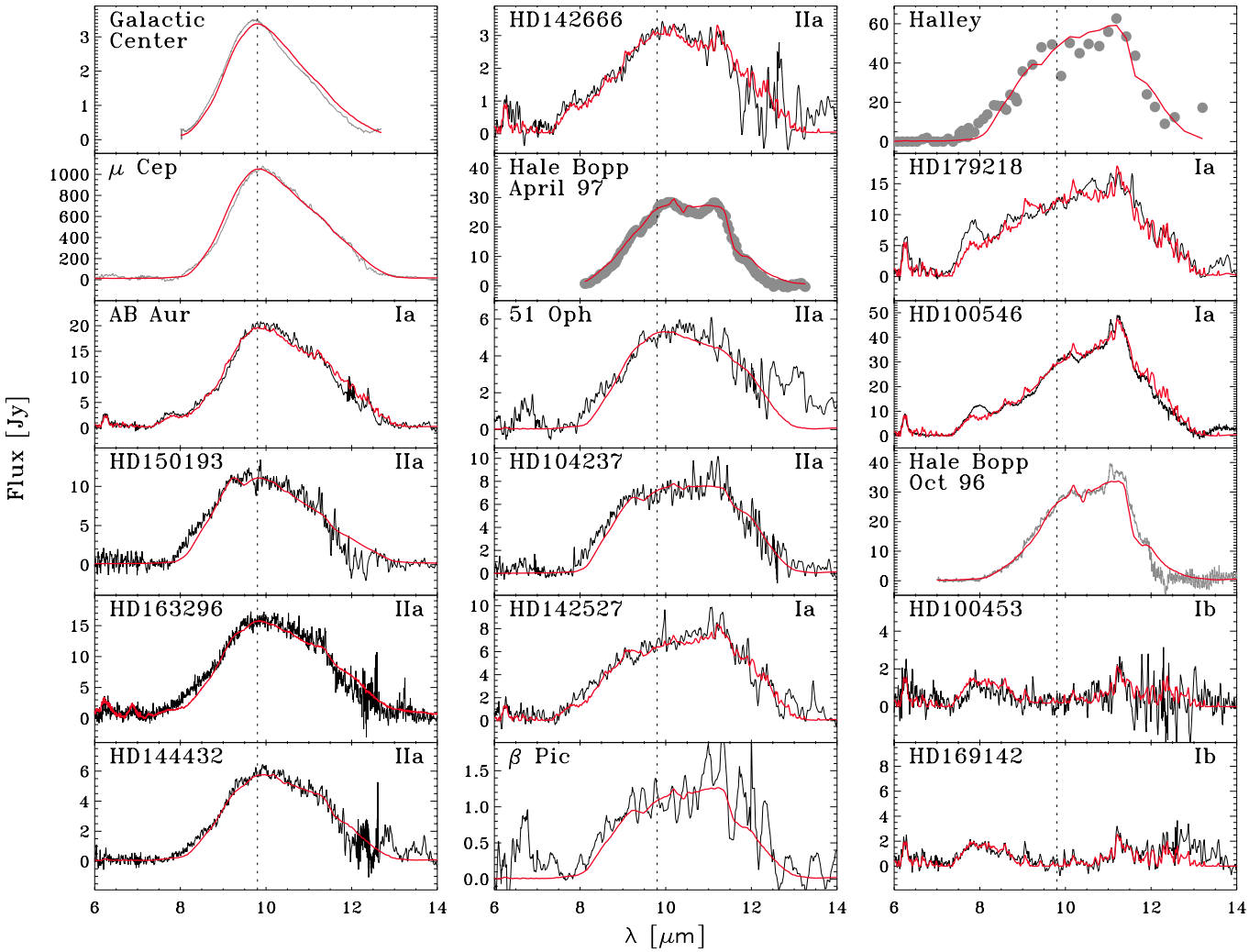

Fig. 4. Fit to the 10 μm silicate feature as observed in our sample of HAEBE stars. Plotted are the continuum subtracted ISO-SWS spectra and our best fit models. Also plotted for reference are the silicate bands of the ISM towards the galactic centre, the red supergiant μ Cep, β Pictoris, and the comets C/1995 O1 (Hale-Bopp) and 1P/Halley. The dashed line indicates the position of the amorphous silicate band as observed for the ISM at 9.8 μm. Indicated in the panels are the group to which the individual systems can be classified on grounds of their overall SED (see Sect. 3.2).

contrast effects with the amorphous silicate and possible confusion with PAH emission at 11.3 μm. Nevertheless, a clear trend can be observed in Fig. 6b. However, we do not find a significant trend if we consider only the HAEBE stars, in contrast with the strong correlation with grain size seen in Fig. 6a. We conclude that for our sample of HAEBE stars the shift in peak position of the silicate feature is due to a change in grain size, while the degree of crystallinity plays only a minor rôle.

Interestingly, this situation seems reversed when we consider β Pic and the two solar system comets in our sample. Figure 6a shows that, considering the correlation with grain size, these objects do not follow the trend set by the HAEBE stars. On the other hand, Fig. 6b indicates that the shift in peak position of the silicate band seen in β Pic and the solar system comets correlates well with the degree of crystallinity. This suggests that for these objects the shift in silicate band position is mainly due to a high fraction of forsterite and is not dominated by grain size effects.

Finally, we note that no correlation between SiO_2 abundance and peak position is evident (Fig. 6c).

Figure 7 shows the same mass ratios plotted against the 8.6 over 9.8 μm flux ratio. No significant correlation can be found with the mass ratio of 2.0 over 0.1 μm amorphous olivine grains or the mass fraction of forsterite. However, a correlation can be observed with the SiO_2 mass ratio. The least square fit results in $b = 1.15 \pm 0.05$ and $a = 0.059 \pm 0.003$.

The relation between the derived mass fractions is presented in Fig. 8. A correlation between the typical grain size of the amorphous olivine and the other dust components is not found as can be seen from Figs. 8a and b. Figure 8c, however, does show a possible correlation between the amount of silica and forsterite. Except for the objects HD 100546 and HD 150193, the HAEBE stars

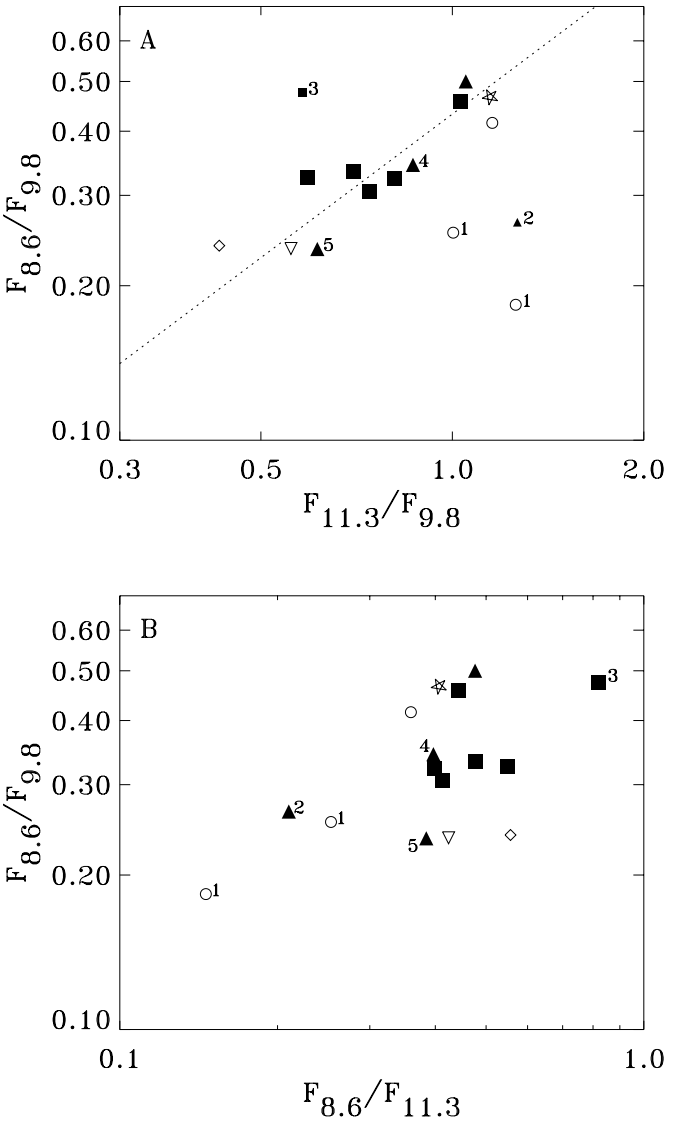

Fig. 5. Color-color diagrams. Plotted are the flux ratios of the excess fluxes at 8.6, 9.8 and 11.3 μm corrected for the PAH emission. The excess flux is the flux minus the assumed continuum at the specified wavelength. The filled symbols indicate the HAEBE stars, the open symbols the reference objects. The HAEBE stars belonging to group Ia are represented by triangles, while those belonging to group IIa are indicated with squares. The diamond, upside down triangle, star, and circles represent the ISM, μ Cep, β Pic, and the solar system comets respectively. The dotted line in the top panel is a least square fit to those HAEBE systems having an 8.6 over 11.3 flux ratio of ∼0.45, indicated with large symbols. A few objects are explicitly marked with a number from 1 to 5, being Hale Bopp, HD 100546, HD 150193, HD 179218, and AB Aur, respectively.

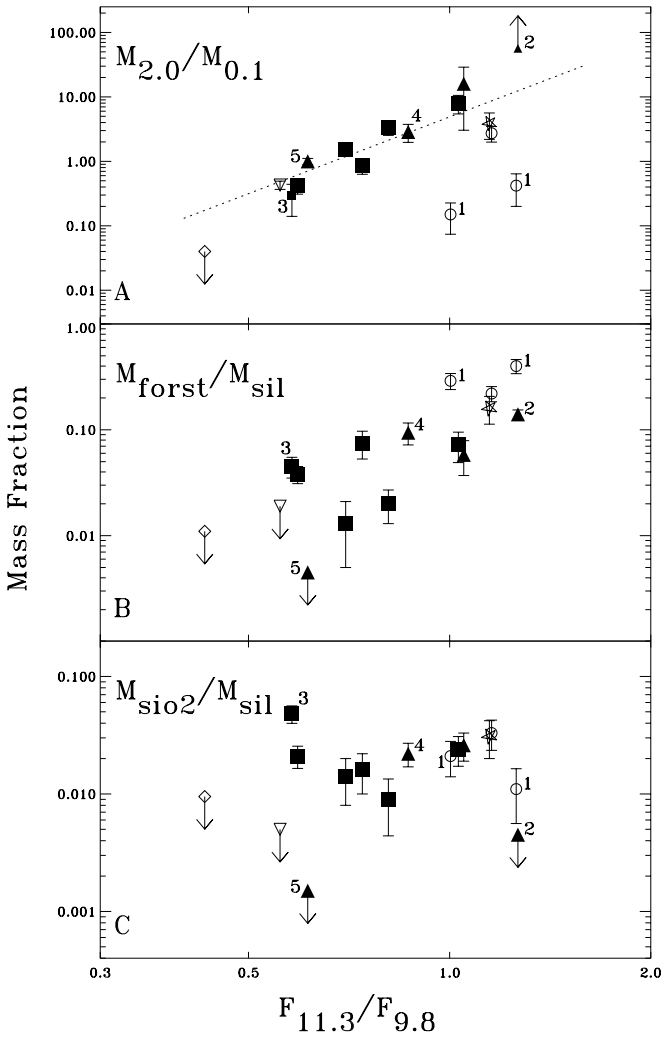

Fig. 6. Correlations between 11.3 over 9.8 μm flux ratio and the derived mass ratios of the dust components. The top panel shows the correlation for the mass ratio between the 2.0 and 0.1 μm amorphous olivine grains. The middle panel shows the mass ratio of forsterite over the total silicate mass, and the bottom panel the SiO_2 mass ratio. The meaning of the symbols is identical as in Fig. 5. The dotted line indicates a least square fit to the HAEBE systems with $F_{8.6}/F_{11.3} \sim 0.45$; these are indicated with large symbols.

seem to have a relatively larger SiO_2 mass fraction with increasing abundances of crystalline magnesium silicates. Again, fitting a relation of the form $Y = aX^b$ to the selected objects, indicated in the figure with large filled symbols, results in $b = 0.47 \pm 0.25$ and $a = 0.082 \pm 0.064$. This is also consistent with the upper limits derived for AB Aur (maked with 5), μ Cep and the ISM, where neither crystalline magnesium silicates or the shoulder at 8.6 μm, indicative for silica, are observed. We note that comet Hale-Bopp also shows a low abundance of SiO_2 despite its high fraction of forsterite. In that sense it strongly resembles HD 100546. Though its $F_{8.6}/F_{11.3}$ flux ratio does not deviate, in the fit we also excluded HD 179218 (marked with 4) due to the detection of enstatite in this system: the derived silica over forsterite mass ratio may not be due to annealing of amorphous iron magnesium silicates, but due to secondary reactions given by Eq. (2) leading to the formation of enstatite. We will discuss this point in detail in Sect. 4.3.

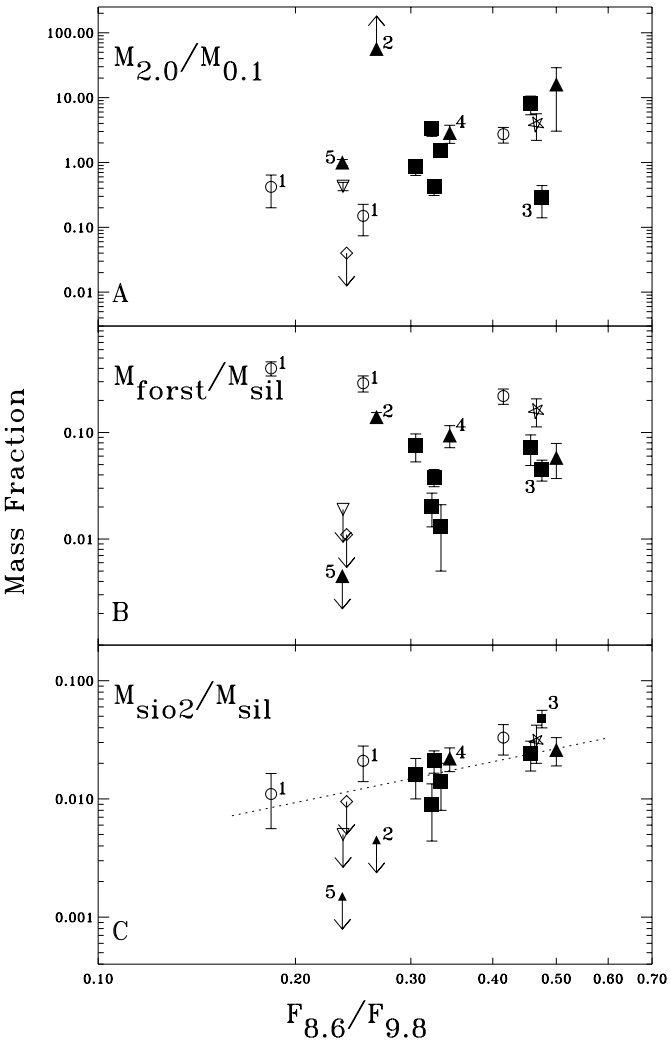

Fig. 7. The correlation between the 8.6 over 9.8 μm flux ratio and the mass ratios of the fitted dust components. For an explanation of the symbols see Fig. 5.

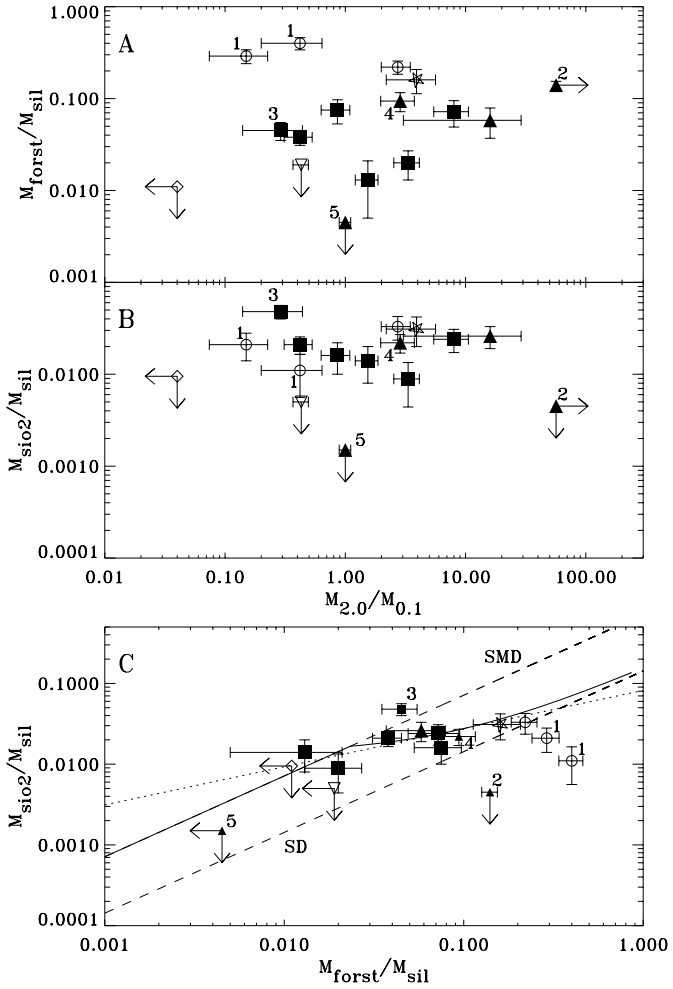

Fig. 8. Correlations between the fitted silicate dust components. **a)** Correlation between the mass ratio of the 0.1 and 2.0 μm sized amorphous olivine grains ($m_{2.0}/m_{0.1}$) and the amount of forsterite. **b)** Correlation between the amount of silica and $m_{2.0}/m_{0.1}$. **c)** Correlation between the mass ratio of silica and the ratio of the crystalline magnesium silicate forsterite. For an explanation of the symbols see Fig. 5. Indicated in Fig. 8c with the dotted line is the fitted correlation of the form $Y = aX^b$. The dashed lines represent the measured annealing behaviour of the amorphous magnesium silicates smectite dehydroxylate (SMD; upper curve) and serpentine dehydroxylate (SD; lower curve). The solid line is the expected annealing behaviour for an initial mixture of 4% of SMD and 96% of SD.

3.2. Correlation to the overall spectral energy distribution

In Paper I we presented a classification of the sample of HAEBE stars discussed here in terms of overall properties of the spectral energy distribution (SED). The SED of so-called Group I sources can be represented by the sum of a power law component and a blackbody component. This blackbody component is needed to account for the large excess group I sources show at far infrared wavelengths. Group II sources only exhibit the power law component. Each of these groups can be further sub-divided into two sub-groups based on the presence of solid state emission, i.e. essentially silicates. If present, the group is given the suffix a, if not present a suffix b is added. This classification on grounds of the overall infrared spectrum is indicated in Figs. 4 through 8. In these figures the filled symbols represent the HAEBE stars. These are further subdivided according to the shape of the SED into triangles (group Ia) and squares (group IIa).

We suggest in Paper I that this classification is linked to the spatial distribution of the dust. Both groups feature an optically thick, geometrically thin disk mid-plane responsible for the power law component. In group I the disk surface is flared, explaining the additional far-IR emission. This group also displays PAH emission, which probably originates in the flaring region that is illuminated by direct stellar UV radiation. It is useful to investigate the relation between the shape of the SED (reflecting the spatial dust distribution) and the shape of the 10 μm feature (reflecting silicate composition). As disks evolve, it is likely that both their geometry and dust composition change.

Looking at Fig. 4, group Ia appears to show the most silicate processing if one excludes AB Aur, which displays the most pristine dust. However, after correction for PAH emission, clear systematic differences between group Ia and IIa cannot be found (cf. Figs. 6 through 8). This suggests that the amount of processing of the silicate grains dominating the mid-IR is *not* correlated to the overall SED and hence not with disk geometry, if the link suggested in Paper I is correct.

Since group Ib shows no solid state features, no information on the amount of grain processing can be derived for this group of stars. A possible explanation for the lack of 10 μm band emission could be the grain size. Grains with sizes much larger than the wavelength at which they radiate (>10 μm) only produce a blackbody continuum. This would imply that group Ib has strongly processed dust compared to ISM material (based on this argument we have placed the two members of this group at end of the sequence in Fig. 4). An alternative explanation could be the absence of a sufficient amount of optically thin material, resulting in a weak or absent silicate band.

4. Discussion

In this section we suggest an explanation for the changes in shape of the 10 μm silicate band, as seen in our sample of 14 Herbig Ae/Be systems, in terms of a simple physical model. The change of the profile is dominated by two effects. First, the peak shifts from 9.8 to 11.3 μm; and second, this shift in peak position is accompanied by the appearance of a broad shoulder shortward of 9.8 μm, extending to about eight micron, which we have characterised using the flux at 8.6 μm.

4.1. Explanation for the change of the 10 μm feature

We have identified two processes that may be responsible for the change in peak position from 9.8 μm, characteristic for ISM material, to 11.3 μm, typical for the solar system comet Hale-Bopp:

1. coagulation of sub-μm sized amorphous olivine grains into micron sized grains; and
2. annealing of amorphous silicates into crystalline magnesium silicates and silica.

The strong correlation between grain size and peak position in HAEBE stars is clearly demonstrated in Fig. 6a, where the flux ratio $F_{11.3}/F_{9.8}$ is shown against the mass ratio of large over small amorphous grains. Larger particles cause an increase of the 11.3 over the 9.8 μm flux. The flux at 11.3 μm also increases when forsterite crystals form from the amorphous iron magnesium silicate dust (Fig. 6b), and seems important for β Pic and the solar system comets, but is not a strong effect in the HAEBE stars. Compared to HAEBE stars with a similar $F_{11.3}/F_{9.8}$ ratio, the former systems show on average a smaller grain size with a larger crystalline silicate fraction.

These observations are consistent with a picture in which grains in HAEBE stars coagulate to form larger grains, *but do not crystallise on the same timescale.* Crystallisation seems to occur on a longer timescale. This is in agreement with a study by Molster et al. (1999b), who analysed the degree of crystallisation and coagulation for long-lived disks surrounding evolved stars. Molster et al. conclude that coagulation precedes crystallisation. As we will discuss in Sect. 4.2, the relation between forsterite and SiO_2 (cf. Fig. 8c) suggests thermal annealing to be responsible for the crystallisation of grains in the HAEBE systems. β Pic and Halley also obey this relation, implying the forsterite found in these objects to have a similar origin. Hale-Bopp and, interestingly, HD 100546 lack SiO_2 emission but do show abundant forsterite indicating a different mechanism may be at work in these objects. In Sect. 4.3.1 we speculate this mechanism may be related to differentiation of large parent bodies. It is important to stress that the HAEBE stars, β Pic, and the comets, lie along a sequence of increasing silicate crystallinity (Fig. 6b). This suggests that processing of silicates starts in the protoplanetary disk and leads to an increased crystallinity. We may conclude that the processes that governed grain processing in the protosolar nebula are also at work in HAEBE stars.

4.2. The chemical composition of the silicate dust

In Fig. 8 we showed that the fraction of SiO_2 tends to increase with the degree of crystallinity. Laboratory studies of thermal annealing of amorphous Mg silicate smokes show an increase in the fraction of forsterite and SiO_2 as a function of time, temperature, or both (Rietmeijer et al. 1986; Hallenbeck & Nuth 1997; Fabian et al. 2000). This implies that the simultaneous occurrence of forsterite and SiO_2 in our sample is consistent with an origin due to thermal annealing in the inner part of the protoplanetary disk. The lack of correlation between grain size and changes in composition supports our previous conclusion that grain growth proceeds independently from these compositional changes.

We point out that the temperature of the grains probed in the 10 μm silicate band (typically 500 K) is well below the annealing temperature of amorphous silicates (about 1100 K). Extrapolation of laboratory experiments indicates that the annealing timescale of such relatively low temperature grains would be prohibitively long compared to the ages of these systems (Hallenbeck et al. 2000). This would imply that in situ formation of the forsterite seen in HAEBE disks is unlikely. Either extrapolation of laboratory results is not permitted and the million year timescale allows for annealing well below the glass temperature, or radial mixing of processed material from the innermost regions is responsible.

Although there is a considerable uncertainty in the relation between silica and forsterite as seen in Fig. 8c, it is in principle possible from the observed trends to set

constraints on the Mg over Si ratio of the amorphous bulk material from which both forsterite and silica are formed during annealing. Here we discuss the principle; more accurate data are needed to provide useful constraints.

To constrain the derived correlation between silica and forsterite we make a comparison with the measured annealing behaviour of amorphous magnesium silicates. Plotted in Fig. 8c are the measured annealing curves of the pure magnesium silicates smectite dehydroxylate (SMD; $Mg_6Si_8O_{22}$) and serpentine dehydroxylate (SD; $Mg_3Si_2O_7$). Condensation experiments show that at low temperatures ($T \sim 500$ K) only these materials are formed (Rietmeijer et al. 1999). Annealing of SMD produces forsterite and silica in a mass ratio of 1.4; for the SD material this ratio is 7.0 (Rietmeijer et al. 2001, in preparation). As one can see, the curves tightly constrain the found correlation. This constrains the Mg/Si ratio between 0.75 (SMD) and 1.5 (SD). The fitted trend implies that with increasing abundance of forsterite the silica over forsterite mass ratio decreases. *This is inconsistent with the annealing of an amorphous material with a homogeneous chemical composition.* Annealing of such a material would give a constant ratio between forsterite and silica. A good match with the observed behaviour is obtained if we adopt a material initially composed of 4% SMD and 96% SD by mass (solid line). In plotting this curve we assume that first all SMD is converted to forsterite and silica, before SD starts to anneal. This difference in annealing time scales is suggested by annealing experiments where the thermal and mineralogical development of the SMD component is found to be ahead of the SD material (Rietmeijer et al. 2001, in preparation). In this way one can produce a flatter curve consistent with the fitted correlation. The bulk Mg/Si ratio of such a composition would be 1.46, which is larger than the solar average bulk composition of CI and CM carbonaceous chondrite of 1.06 and 1.04 respectively (Brownlee 1978). However, it is more consistent with the interstellar value adopted by Snow & Witt (1996) of 1.34. This latter value is based on a compilation of stellar composition data of both field and cluster B and disk F and G stars. The data show that the abundances of young stars deviate considerably from solar. The authors argue that this deviation could reflect the enhancement of the proto-solar cloud abundances by a nearby supernova event (e.g. Cameron & Truran 1997; Olive & Schramm 1982).

In the discussion above we used the results of annealing experiments of pure magnesium silicates. This is motivated by ISO observations which show that the crystalline silicates contain little or no iron. It is, however, likely that the amorphous material will contain iron. If so, this could have consequences for the interpretation of the Mg/Si ratio derived above. An important question is how iron is incorporated into the amorphous silicate. This is hard to determine observationally due to the amorphous structure of the silicate. The iron could be in a solid solution or consist of a mix of pure magnesium and pure iron silicates. If forsterite and silica are formed through the annealing of Fe-containing amorphous material, the iron somehow has to be removed from the lattice in the annealing process, forming metallic iron or iron oxides depending on the oxygen partial pressure. During this solid state reduction of iron the Mg/Si ratio does not change and the value derived above would consequently imply a non-solar composition.

Condensation experiments (Rietmeijer et al. 1999) favor the possibility that the amorphous material consists of a mixture of pure iron and pure magnesium silicates. If this is so, the derived Mg/Si ratio could only be relevant to the amorphous magnesium silicates. Annealing experiments by Hallenbeck et al. (2000) show that the annealing time scales for iron silicates are considerably longer than for magnesium silicates. It could well be that while the magnesium silicates anneal and form forsterite and silica, the iron silicates stay amorphous. Given a system where the amorphous magnesium silicates have a Mg/Si ratio of 1.46, if the amorphous iron silicates would contain ∼30% of the total amount of Si available in this system, the bulk Mg/Si ratio would be solar. We stress however that the uncertainties on the derived bulk Mg/Si ratio do not allow us to decide whether or not it deviates from Solar.

4.3. Deviating objects

From our sample of HAEBE stars, three objects deviate in dust composition from the other systems: HD 100546 and HD 150193, having a lower respectively larger SiO_2 mass fraction compared with the amount of forsterite in these systems and HD 179218 which is the only system that shows emission from enstatite. In addition, comet Hale-Bopp deviates in a way which strongly resembles HD 100546. We discuss these objects below.

4.3.1. HD 100546 and Hale-Bopp

The mineralogical composition of the silicate dust in HD 100546 is strongly deviant from most other HAEBE stars: it has very abundant cool crystalline silicates (Malfait et al. 1998). Our analysis indicates that the ratio of forsterite over amorphous silicates at temperatures dominating the 10 μm region is *lower* than that of the cooler material dominating at longer wavelengths. We also find a lack of 8.6 μm SiO_2 emission. This suggests that thermal annealing may not have been the origin of the forsterite in HD 100546.

A high fraction of forsterite is also apparent in comet Hale-Bopp (see also Crovisier et al. 1997). As in HD 100546, SiO_2 is under abundant relative to forsterite. It is tempting to speculate on the origin of this behaviour. One intriguing possibility is that (part of) the grains in HD 100546 and Hale-Bopp are *second generation*, i.e. originate from larger parent bodies – in which substantial alteration of the silicates occurred – that were destroyed through collisions. The recent discovery of gas in the disk of β Pic (Thi et al. 2001) shows that collisional processes can dominate in disks still containing some gas. Possibly,

second generation dust can also be produced in the disk of HD 100546. The high fraction of forsterite in comet Hale-Bopp certainly rules out the possibility that it was formed from pristine ISM dust, and hence is strong proof that comets contain material processed in the proto-solar nebula. This processing could either be thermal annealing (Halley) or crystallisation by inclusion into a large parent body (Hale-Bopp).

It a separate paper we will extensively discuss the dust composition of HD 100546 and compare it to Hale-Bopp and other solar system comets (Bouwman et al. 2001, in preparation).

4.3.2. HD 150193

It is not clear why HD 150193 has such a high abundance of SiO_2. We are confident of the identification of the 8.6 and 20 μm emission with SiO_2 given the quality of the spectral match (Fig. 1). A large amount of silica can form from an amorphous silicate by annealing if the Mg/Si ratio is lower than derived for the other systems. We can only speculate on why this should be the case. We note that HD 150193 is the only known binary in our sample. A binary companion can limit the disk size and accretion and can cause the disk to empty out at much shorter time scales (Calvet et al. 2000). Also the settling and growth of grains can be prevented (Sato & Nakagawa 2000). Indeed, HD 150193 shows the smallest grains producing the silicate feature and has a large inner hole of about 0.6 AU (Millan-Gabet et al. 2001). This is much larger than observed for AB Aur and HD 163296, which have similar stellar ages (van den Ancker et al. 1998) suggesting that indeed the protoplanetary disk in HD 150193 is influenced by the companion star.

4.3.3. HD 179218

From the ISO spectra, no conclusive evidence for the presence of enstatite in HAEBE systems can be found except for one system, HD 179218. This is the only system in which large quantities of enstatite have formed. Annealing experiments of a magnesium silicate smoke done by Rietmeijer et al. (1986) show that the initially formed forsterite and silica react and form enstatite by the following reaction

$$Mg_2SiO_4 + SiO_2 \longrightarrow 2MgSiO_3. \quad (2)$$

It is unclear why this reaction has not taken place in the other systems. The formation of enstatite depends on the amount of reaction surface between the forsterite and silica units. The dust particles must be reasonably compact for this reaction to occur on time scales comparable with the evolutionary time scales of the HAEBE systems. An aggregate can be compressed during collisions if the relative velocities are close to the destruction velocities (Dominik & Tielens 1997). These velocities, however, are only reached with low gas densities when the coupling between the gas and dust becomes inefficient. We note that with $L{\sim}300\ L_\odot$ HD 179818 stands out by about an order of magnitude compared to the other stars in our sample. This large luminosity can influence the disk structure through radiation pressure forces and may lead to the dispersal of the gas at much shorter time scales compared to the other HAEBE stars. This clearing out of material is evidenced by interferometric observations showing an inner hole of ∼1 AU (Millan-Gabet et al. 2001), which is larger than for any of the other systems investigated here for which such observations are available.

5. Conclusions

The results of this study can be summarized as follows:

1. The observed 10 μm silicate bands in the ISO spectra of the studied HAEBE systems can be ordered from a profile peaking at 9.8 μm – resembling the ISM silicate band – towards a profile similar to cometary spectra, peaking at 11.3 μm. We find a relation between the 11.3 μm flux and the occurrence of a broad shoulder at ∼8.6 μm.
2. We can model the different 10 μm silicate profiles using three components:
   - silica (SiO_2), responsible for the 8–9 μm blue shoulder in the silicate band;
   - forsterite, contributing at 11.3 μm; and
   - amorphous olivine with two typical grain sizes of 0.1 and 2.0 μm.
3. We identify two main causes for the observed shift in peak position of the silicate band:
   - a change in average grain size from small (0.1 μm) to large (2 μm). This is the result of the depletion of small grains in the inner region of the disk, due to coagulation or other effects that preferentially remove small grains;
   - a change in composition from amorphous silicate to a mixture of amorphous and Mg-rich crystalline silicate (forsterite). This may be the result of thermal annealing in the inner regions of the disk. Laboratory experiments indicate that thermal annealing produces both crystalline silicates and SiO_2.
4. The change in shape of the 10 μm silicate band in HAEBE stars is mainly due to an increase in average grain size of the dust.
5. The HAEBE stars, β Pic and the solar system comet Halley form a sequence of increasing silicate crystallinity. As the degree of crystallinity increases, the abundance of SiO_2 also tends to increase. This is consistent with the expected changes in composition resulting from thermal annealing of amorphous silicates in the inner regions of the proto-planetary disk.
6. The observed relation between silica (SiO_2) and forsterite abundance implies that the composition of the amorphous silicate from which these materials are formed can not be chemically homogeneous.

A combination of smectite (4% by mass) and serpentine (96%) gave a good fit result.

7. The mineralogy of HD 100546 and comet Hale-Bopp is remarkable, with very high forsterite abundance and no evidence for SiO_2 (cf. Crovisier et al. 1997; Malfait et al. 1998). This composition, which deviates from that of the other objects, suggests a different origin for the forsterite, possibly from the destruction of highly differentiated large parent bodies. Two other objects, HD 150193 and HD 179218 show very high SiO_2 and enstatite abundances, respectively. The origin of these deviating mineralogies is not well understood.
8. Crystallisation timescales appear to be longer than coagulation timescales.
9. No correlation between dust composition and disk geometry can be observed.

Acknowledgements. The authors would like to thank the referee J. Mathis, for helpful comments that have improved this paper, and F. J. M Rietmeijer for constructive discussions. The authors would like to acknowledge the financial support from NWO *Pionier* grant 600-78-333. AdK also gratefully acknowledges support from NWO Spinoza grant 08-0 to E. P. J. van den Heuvel.

References

Allamandola, L. J., Tielens, G. G. M., & Barker, J. R. 1989, ApJS, 71, 733
Allen, C. C., Morris, R. V., Lauer, H. V. Jr., & McKay, D. S. 1993, ICARUS, 104, 291
Aumann, H. H., Beichman, C. A., Gillett, F. C., et al. 1984, ApJ, 278, 23
Beust, H., Lagrange, A.-M., Plazy, F., & Mouillet, D. 1996, A&A, 310, 181
Bohren, C. F., & Huffman, D. R. 1983, Absorption and Scattering of Light by Small Particles (John Wily & Sons Inc.)
Bouwman, J., de Koter, A., van den Ancker, M. E., & Waters, L. B. F. M. 2000, A&A, 360, 213
Bregman, J. D., Witteborn, F. C., Allamandola, L. J., et al. 1987, A&A, 187, 616
Brownlee, D. E. 1978 Protostars and Planets, ed. T. Gehrels (University of Arizona Press), 134
Calvet, N., Hartmann, L., & Strom, S. E. 2000, Protostars and Planets IV, ed. V. Mannings, A. P. Boss, & S. S. Russell (University of Arizona Press), 377
Cameron, A. G. W., & Truran, J. W. 1977, Icarus, 30, 447
Clegg, P. E., Ade, P. A. R., Armand, C., et al. 1996, A&A, 315, 38
Crovisier, J., Leech, K., Bockelee-Morvan, D., et al. 1997, Sciences, 275, 1904
de Graauw, T., Haser, L. N., Beintema, D. A., et al. 1996, A&A, 315, L49
Dominik, C., & Tielens, A. G. G. M. 1997, ApJ, 480, 647
Dorschner, J., Begemann, B., Henning, Th., Jäger, C., & Mutschke, H. 1995, A&A, 300, 500
Dunkin, S. K., Barlow, M. J., Ryan, & Sean, G. 1997, MNRAS, 286, 604
Fabian, D., Jäger, C., Henning, Th., Dorschner, J., & Mutschke, H. 2000, A&A, 364, 282
Grady, C. A., Sitko, M. L., Bjorkman, K. S., et al. 1997, ApJ, 483, 449
Grady, C. A., Pérez, M. R., Bjorkman, K. S., & Massa, D. 1999, ApJ, 511, 925
Gray, R. O., & Corbally, C. J. 1998, AJ, 116, 2530
Guillios, O., Nenner, I., Papoular, R., & Reynaud, C. 1996, ApJ, 464, 810
Hallenbeck, S. L., & Nuth, J. A. 1997, Ap&SS, 255, 427
Hallenbeck, S. L., Nuth, J. A., & Nelson, R. N. 2000, ApJ, 535, 247
Hayward, T. L., Hanner, M. S., & Sekanina, Z. 2000, ApJ, 538, 428
Jäger, C., Molster, F. J., Dorschner, J., et al. 1998, A&A, 339, 904
Kessler, M. F., Steinz, J. A., Anderegg, M. E., et al. 1996, A&A, 315, 27
Kukarkin, B. V., Kholopov, P. N., Pskovsky, Y. P., et al. 1971, General Catalogue of Variable Stars, 3rd ed.
Malfait, K., Bogaert, E., & Waelkens, C. 1998a, A&A, 331, 211
Malfait, K., Waelkens, C., Waters, L. B. F. M., et al. 1998b, A&A, 332
Malfait, K., Waelkens, C., Bouwman, J., de Koter, A., & Waters, L. B. F. M. 1999, A&A, 345, 181
Mannings, V., & Sargent, A. I. 1997, ApJ, 490, 792
Mannings, V., & Sargent, A. I. 2000, ApJ, 529, 391
Meeus, G., Waters, L. B. F. M., Bouwman, J., et al. 2001, A&A, 365, 476
Millan-Gabet, R., Schloerb, F. P., & Traub, W. A. 2001, ApJ, 546, 358
Molster, F. J., Waters, L. B. F. M., Trams, N. R., et al. 1999a, A&A, 350, 163
Molster, F. J., Yamamura, I., Waters, L. B. F. M., et al. 1999b, Nature, 401, 563
Olive, K. A., & Schramm, D. N. 1982, ApJ, 257, 276
Pantin, E., Waelkens, C., & Malfait, K. 1999, in The Universe as Seen by ISO. ESA-SP 427, ed. P. Cox, & M. F. Kessler, 385
Rietmeijer, F. J. M., Nuth, J. A., & Mackinnon, I. D. R. 1986, Icarus, 65, 211
Rietmeijer, F. J. M. 1988, Proc. 19th Lunar Planet. Sci. Conf., 513
Rietmeijer, F. J. M., Nuth, J. A., & Karner, J. M. 1999, ApJ, 527, 395
Sato, Y., & Nakagawa, Y. 2000, IAUS, 202, 83
Servoin, J. L., & Piriou, B. 1973, Phys. Stat. Sol. (b), 55
Snow, T. P., & Witt, A. N. 1996, ApJ, 468, L65
Spitzer, W. G., & Kleinman, D. A. 1961, Phys. Rev., 121, 1324
Thi, W. F., Blake, G. A., van Dishoeck, E. F., et al. 2001, Nature, 409, 60
van den Ancker, M. E., de Winter, D., Tjin, A., & Djie, H. R. E. 1998, A&A, 330, 145
van den Ancker, M. E., Bouwman, J., Wesselius, P. R., Waters, L. B. F. M., & van Dishoeck, E. F. 2000, A&A, 357, 325
Waters, L. B. F. M., & Waelkens, C. 1998, ARA&A, 36, 233